Journal of the Taiwan Institute of Chemical Engineers 150 (2023) 105042

Contents lists available at ScienceDirect

Journal of the Taiwan Institute of Chemical Engineers

journal homepage: www.journals.elsevier.com/journal-of-the-taiwan-institute-of-chemical-engineers

Hollow-architected Co_3O_4 for enhancing Oxone activation to eliminate an anesthetic, benzocaine, from water: A structure-property investigation with degradation pathway and eco-toxicity

Xin-Yu Jiang [a], Young-Kwon Park [b], Jet-Chau Wen [c], Ha Manh Bui [d], Yi-Feng Lin [e,*], Sanya Sirivithayapakorn [f], Ta Cong Khiem [a], Venkata Subbaiah Munagapati [c], Kun-Yi Andrew Lin [a,g,*]

[a] Department of Environmental Engineering & Innovation and Development Center of Sustainable Agriculture, National Chung Hsing University, 250 Kuo-Kuang Road, Taichung, Taiwan
[b] School of Environmental Engineering, University of Seoul, Seoul 02504, Republic of Korea
[c] National Yunlin University of Science and Technology, Douliu, Yunlin County, Taiwan
[d] Faculty of Environment, Saigon University, Ho Chi Minh 70000, Viet Nam
[e] Department of Chemical Engineering and R&D Center for Membrane Technology, Chung Yuan Christian University, 200 Chung Pei Rd., Chungli, Taoyuan, Taiwan
[f] Environmental Engineering Department, Faculty of Engineering, Kasetsart University, Bangkok, Thailand
[g] Institute of Analytical and Environmental Sciences, National Tsing Hua University, Hsinchu, Taiwan

ARTICLE INFO

Keywords:
Hollow Co_3O_4
Oxone activation
Benzocaine degradation
SR-COTs

ABSTRACT

Background: As the most widely-used oral anesthetic, benzocaine (BZC), is increasingly detected in municipal wastewater and regarded as an emerging contaminant. Thus, it would be highly imperative to develop useful methods to eliminate BZC from water. However, very few studies have been ever reported, and only photocatalysis of BZC was attempted. Therefore, this present study aims to be the first study of developing the sulfate-radical-based chemical oxidation technology (SR-COT) for degrading BZC.

Methods: For establishing a useful SR-COT, the oxidant, Oxone, is then adopted and a facile nanostructured Co_3O_4 is then developed for maximizing catalytic activities of Oxone activation by creating a hollow fluffy Co_3O_4 nanostructure using CoMOF as a template, followed by a carving-architected treatment to afford the hollow fluffy Co_3O_4 (HFCC).

Significant findings: In comparison to the solid (non-hollow) Co_3O_4 (SCC), HFCC possesses not only the excellent textural properties, but also superior electrochemical properties and highly reactive surfaces, making HFCC exhibit the significantly higher catalytic activity than SCC as well as traditional Co_3O_4 nanoparticle in activating Oxone to degrade BZC. The density function theory calculation is performed to investigate the degradation pathway, and the corresponding eco-toxicity is also studied to realize the degradation implication of BZC by HFCC-activated Oxone.

1. Introduction

Benzocaine (BZC) is also the most common over-the-counter oral drug for relieving oral pains, making it an essential pharmaceutical and personal care product. The extensive consumption of BZC has increased the presence of BZC in wastewater [1]; unfortunately, BZC is validated to exhibit many adverse effects, making BZC an emerging contaminant [1]. While BZC is increasingly detected in wastewater, very few studies have been conducted to eliminate BZC from water except for those on photocatalysis [2,3], sorption [4], and filtration [5]. While photocatalysis might be feasible for degrading BZC, sulfate-radical-based chemical oxidation technologies (SR-COTs) receive increasing favors for treating emerging contaminants as SR can exhibit higher redox potentials (E_0 of $SO_4^{\bullet-}$ = 2.5–3.1 V vs NHE), making SR-COTs a promising approach for eliminating BZC. However, no existing studies have been ever conducted of developing SR-COTs for degrading BZC.

Thus, the aim of this study would attempt to develop useful a SR-COT to treat BZC in water.

* Corresponding authors.
E-mail addresses: yflin@cycu.edu.tw (Y.-F. Lin), linky@nchu.edu.tw (K.-Y.A. Lin).

https://doi.org/10.1016/j.jtice.2023.105042
Received 7 March 2023; Received in revised form 10 July 2023; Accepted 11 July 2023
Available online 4 August 2023

For producing SR, the oxidant, Oxone, is a popular precursor reagent; however, Oxone must be activated for quickly releasing SR and other derivative reactive oxygen species (ROS). Therefore, for successfully eliminating BZC from water using Oxone-based SR-COT, a useful and effective activator must be required [6,7]. Because cobaltic catalysts have been proven to be the most useful materials for Oxone activation in water [7–10], and no literature has ever been reported for using Co-activated Oxone for BZC degradation, it is imperative for establishing useful Co-based materials to optimize Oxone activation in BZC degradation.

Conventionally, Co_3O_4 is proven as a useful heterogeneous catalyst for activating Oxone [11,12]; however, Co_3O_4 NPs tend to aggregate, even in aqueous solutions [13]. Given that textural characteristics (i.e., surface areas and porosities) and surface chemistry are major factors to determine activities of heterogeneous catalysts, recently, hollow-architected nanomaterials have received increasing favors because the hollow configuration exhibits higher contact areas and porosities without redundant weights. Besides, the hollow structure would also configure Co_3O_4 NPs into a well-defined shape to avoid aggregation. Therefore, it would be advantageous to fabricate such a hollow-structured Co_3O_4 for activating Oxone to degrade BZC.

To this end, the present study offers a facile method for fabricating

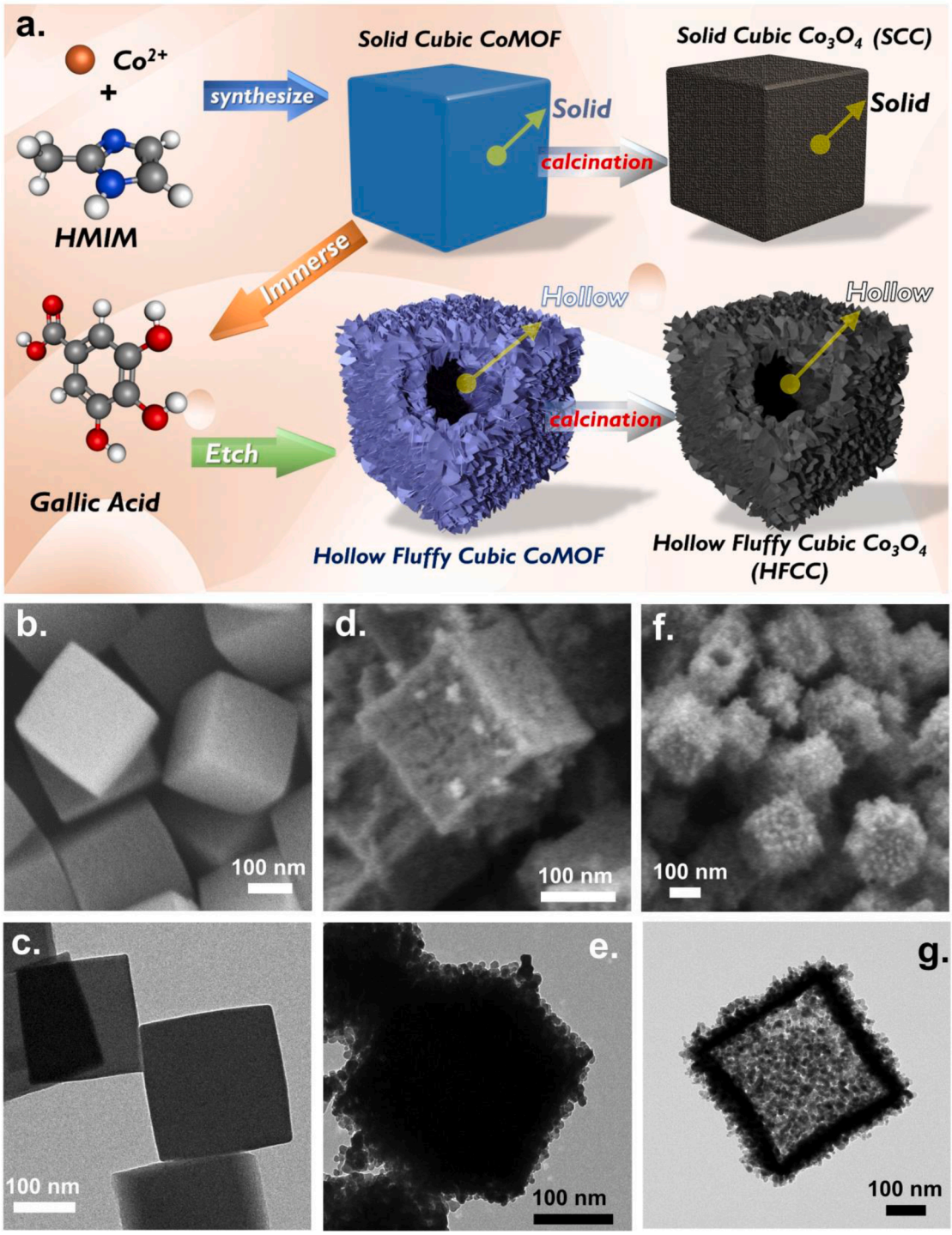

Fig. 1. (a) Preparation scheme of HFCC from CoMOF; images of (b, c) CoMOF, (d, e) SCC, and (f, g) HFCC.

such a hollow-structured Co_3O_4 by using a cubic Co-based metal organic framework (CoMOF) as a template, which would be then chemically-carved using a plant extract, gallic acid (GA), and subsequently calcined, for architecting a unique hollow and fluffy cubic Co_3O_4 (HFCC). Moreover, an analogue to HFCC without the hollow structure as a solid cubic Co_3O_4 (SCC) would be also fabricated for comparing with HFCC to investigate the structure-property relationship. More importantly, the corresponding degradation pathway of BZC by HFCC/Oxone is also explored using experimental analysis and computer-aided investigations; the eco-toxicity evaluation of the possible intermediates would be also performed.

2. Experimental

2.1. Catalyst preparation

Carving-architected hollow fluffy cubic Co_3O_4 (HFCC) was prepared as illustrated in Fig. 1(a). Firstly, the CoMOF was first prepared using the previously-reported method [14–16]. Then, 200 mg CoMOF were soaked in 200 mL of DI water/95% ethanol (v/v = 1/1) and 200 mg GA for 10 min. The time of the carving treatment would have a great effect on the resultant structure of the product. The longer the time is, the hollower the structure becomes until at some point it would completely vanish by the carving effect of gallic acid. Since our goal was to produce the hollow-structured Co_3O_4 (i.e., the interior was void and the outer layers were remained). According to our investigations by changing times, we found that 10 mins would be an ideal duration for the carving treatment in order to afford such as hollow structure. Anytime longer than 10 min would over-etch CoMOF, whereas anytime shorter than 10 min would not create enough internal spaces in CoMOF. The resultant carved product was centrifuged, rinsed with ethanol, and dried at 65 °C, followed by calcination at 600 °C in the air for 4 h to afford HFCC. The solid nanocuble (NC) of Co_3O_4 (denoted as SCC) was prepared by directly calcining the solid CoMOF NC without the carving treatment using the same calcination condition as above.

2.2. BZC degradation procedure

BZC degradation was conducted in a 100 mL glass beaker containing 100 mL of 10 μM BZC under stirring at 30 °C without pH adjustment. The reaction took place after adding 2.5 mg HFCC followed by 20 mg Oxone. Aliquot was taken out periodically and passed through a filter (PVDF, 0.22 μm). The BZC conc. was measured with an UV–vis spectrophotometer at 275 nm. The effects of different parameters (catalyst/Oxone dosages, temperatures, pH, waters, anions, and inhibitors) on BZC degradation were examined by repeating the same procedure but changing the specific parameters to the target values for catalyst/Oxone dosages, temperatures, and pH before reaction. For waters, DI water was replaced with tap water and seawater. Meanwhile, effects of anions and inhibitors were examined by adding their specific amount along with BZC to the solution.

The degradation kinetics of BZC was analyzed by employing the pseudo-first-order reaction:

$$Ln(C_t / C_0) = -kt \quad (1)$$

In reusability test, the experiment was conducted as abovementioned but the scale was multiplied by ten times to prevent catalyst loss. The catalyst-containing solution after reaction was filtered with a 0.45 μm filter paper and washed with EtOH/DI water between cycles before being dried at 65 °C for 1 h. The decomposition of Oxone was conducted using the same procedure as that used for BZC degradation but the solution in this case was DI water. Total organic carbon was analyzed using total organic carbon analyzer (Shimadzu TOC-VSH, Japan).

3. Results and discussion

3.1. Characterizations

CoMOF with cubic configuration and the solid texture were first observed in Fig. 1((b and c)). After calcination, the overall configuration was still preserved but the surface became roughened (Fig. 1(d and e)). On the other hand, when CoMOF underwent the carving treatment, GA reacted partly with Co^{2+} released outwards and on the surface to result in hollow configuration with cubic structure and fluffy appearance of HFCC after calcination (Fig. 1(f and g)).

The XRD of CoMOF in Fig. 2a were properly-indexed to simulated ZIF-67 [17], validating the successful formation of CoMOF. Meanwhile, that of SCC and HFCC afforded a series of peaks ascribed to Co_3O_4 (JCPDS#43–1003), indicating that the form of Co_3O_4 in HFCC and SCC was a spinel structure [18], suggesting the solid cubic Co_3O_4 and hollow fluffy cubic Co_3O_4, respectively. Fig. 2(b) exhibited the elemental constituents of SCC and HFCC were merely Co and O, confirming the successful preparation of SCC and HFCC.

Fig. 2(c) reveals the amount of N_2 sorption to HFCC was high with a hysteresis loop, indicating that HFCC would exhibit a high surface area with a large porosity, particularly mesopores as displayed in Fig. 2(d). The surface area of HFCC was 66 cm^2/g with a porosity as 0.39 cc/g. Nonetheless, the amount of N_2 adsorbed to SCC was significantly less as shown in Fig. 2(c); therefore, SCC only showed 36 m^2/g with a porosity of 0.25 cc/g. These comparisons also confirm that the carving treatment would enable HFCC for revealing a much more advantageous textural properties, especially the porous structure, which would maximize its active surface for catalytic activation of Oxone. The traditional Co_3O_4 NP was also employed here for comparisons and its N_2 sorption was extremely low as shown in Fig. 2(c) with the significantly low pore volume (Fig. 2d). Therefore, the surface area of Co_3O_4 NP was merely 2 m^2/g with 0.01 cc/g, possibly because these Co_3O_4 NPs were seriously aggregated as shown in Fig. S6.

Fig. 2(e) displayed Raman spectra of HFCC, SCC, and Co_3O_4 NP. All of these were comprised of similar patterns with noticeable bands at 192, 474, 515, 613 and 680 cm^{-1}, attributed to the F^1_{2g}, E_g, F^2_{2g}, F^3_{2g}, *and* A_{1g} of Raman active vibration modes in Co_3O_4 [19–21]. Three F_{2g} peaks are associated with characteristics of tetrahedral (CoO_4) sites, while A_{1g} is related to characteristics of octahedral (CoO_6) sites [22]. Fig. 2(f) further displays that the A_{1g} band of Co_3O_4 NP centered at 682 cm^{-1}; however, the center of the band in SCC had shifted from 680 cm^{-1} to 678 cm^{-1} and the band center in HFCC even changed to 676 cm^{-1}. On the other hand, the similar band shift had been also observed in the case of F^1_{2g} as shown in Fig. 2(g). As the band center of Co_3O_4 NP was at 197 cm^{-1}, the F^1_{2g} band center of SCC shifted to the lower location to 194 cm^{-1}. The corresponding band center of HFCC had further changed to 190 cm^{-1}. As these Raman bands are reported to involve the oxygen mobility in metal oxides [23]; the band shifts from the higher position of Co_3O_4 NP to the lower position of SCC and even HFCC signifies that Co_3O_4 from calcination of CoMOF might exhibit a higher degree of defects, and HFCC seemed to contained even more defects than SCC as well as Co_3O_4 NP. This feature might enable HFCC to reveal more catalytic active surfaces [24], that would possibly improve catalytic activities of Oxone activation. Similar results can be also observed in the temperature-programmed reduction analysis (Fig. 2(h, i)) (the detailed discussion is in the Supporting Information).

3.2. BZC degradation

BZC degradation using Oxone activated by HFCC was evaluated in Fig. 3(a). Nevertheless, since it was possible that BZC might be removed via adsorption, the adsorption of BZC onto HFCC was investigated. In Fig. 3(a), the BZC concentration was almost no change in the presence of HFCC, signifying that BZC could not be eliminated by adsorption. Moreover, when Oxone alone was used, BZC was barely eliminated in

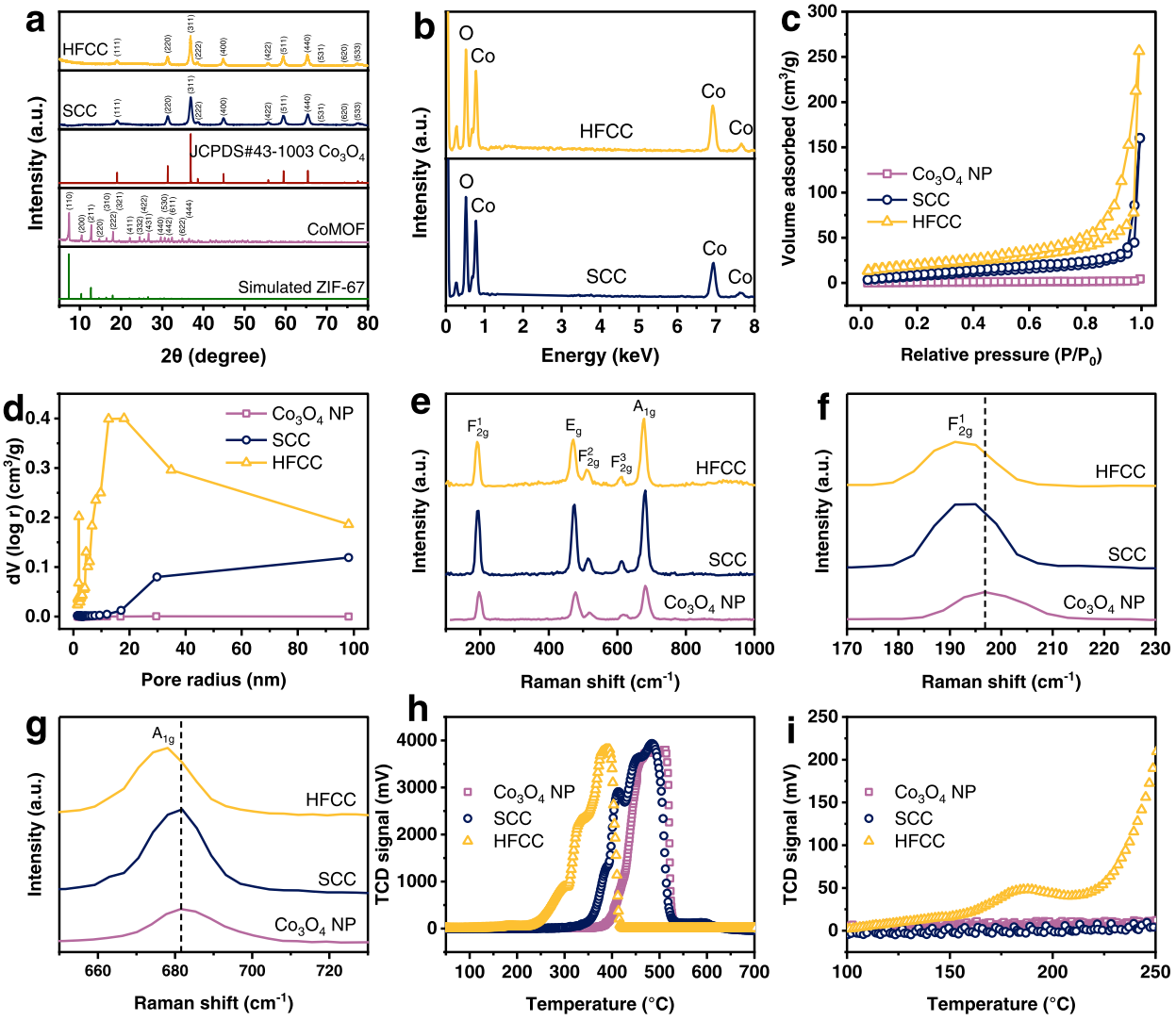

Fig. 2. Characterizations of Co_3O_4 NP, SCC, and HFCC: (a) XRD patterns, (b) EDS spectra, (c) N_2 sorption isotherms, (d) pore size distributions, (e-g) Raman spectra, (h, i) H_2-TPR profiles.

30 min, indicating that Oxone without activation would not efficiently eliminate BZC. However, when both of HFCC and Oxone were combined, BZC concentration was quickly reduced and completely removed as its C_t/C_0 reached "0″ in 30 min, suggesting that HFCC seemed capable of activating Oxone to degrade BZC in water. For comparison, traditional Co_3O_4 NP and SCC were also adopted to activate Oxone for degrading BZC in Fig. 3(a). Co_3O_4 NP/Oxone enabled C_t/C_0 in 30 min to reach 0.78 (i.e., 22% of BZC removed), whereas SCC/Oxone led to C_t/C_0 = 0.5 in 30 min. These cobaltic catalysts were ascertained to activate Oxone for BZC degradation; however, the BZC degradation efficiencies of Co_3O_4 NP and SCC seemed noticeably lower than that of HFCC. Removal of total organic carbon (TOC) of BZC degradation by HFCC-activated Oxone as well as SCC-activated Oxone was also examined as shown in Fig. S7. Within 30 min, ~67% of TOC was removed by HFCC-activated Oxone during BZC degradation, whereas a relatively low TOC removal (~36%) was achieved by SCC-activated Oxone. These results demonstrated that BZC was assuredly degraded and partially mineralized by Oxone and HFCC enabled a noticeably higher TOC removal than SCC.

To further quantitatively compare performances of these catalysts for BZC degradation, the pseudo first order reaction kinetics was then employed and the corresponding rate constants of BZC degradation are summarized in Fig. 3(b). The rate constant (k) by HFCC/Oxone is 0.1321 min^{-1}, which was considerably larger than those of Co_3O_4 NP/Oxone (0.0259 min^{-1}) and SCC/Oxone (0.0528 min^{-1}), confirming the advantageous catalytic activity of HFCC over Co_3O_4 NP and SCC.

In view of the much faster BZC degradation by HFCC, it would be interesting to further probe into Oxone consumption by HFCC in comparison with other catalysts [20]. Thus, the variation of Oxone concentration during BZC degradation was then analyzed in Fig. 3(c). The Oxone concentration with HFCC reduced rapidly during BZC degradation as ~85% of Oxone had been decomposed by HFCC in 30 min. On the contrary, the Oxone concentration during BZC degradation by SCC seemed much slower. The corresponding k of Oxone consumption by both of catalysts are displayed in Fig. 3(d) and the k using HFCC was determined as 0.0595 min^{-1}, whereas the k by SCC was much smaller as 0.0138 min^{-1}, validating that the Oxone consumption by HFCC seemed much more effective and faster than SCC, thereby enabling the faster BZC degradation.

Since Oxone activation involves redox reactions between Oxone and activators, electrochemical properties of catalysts shall play crucial roles in Oxone activation [9]. As HFCC showed a significantly higher catalytic activity than SCC for degrading BZC, it was informative to examine electrochemical differences between HFCC and SCC. Fig. 4(a) firstly

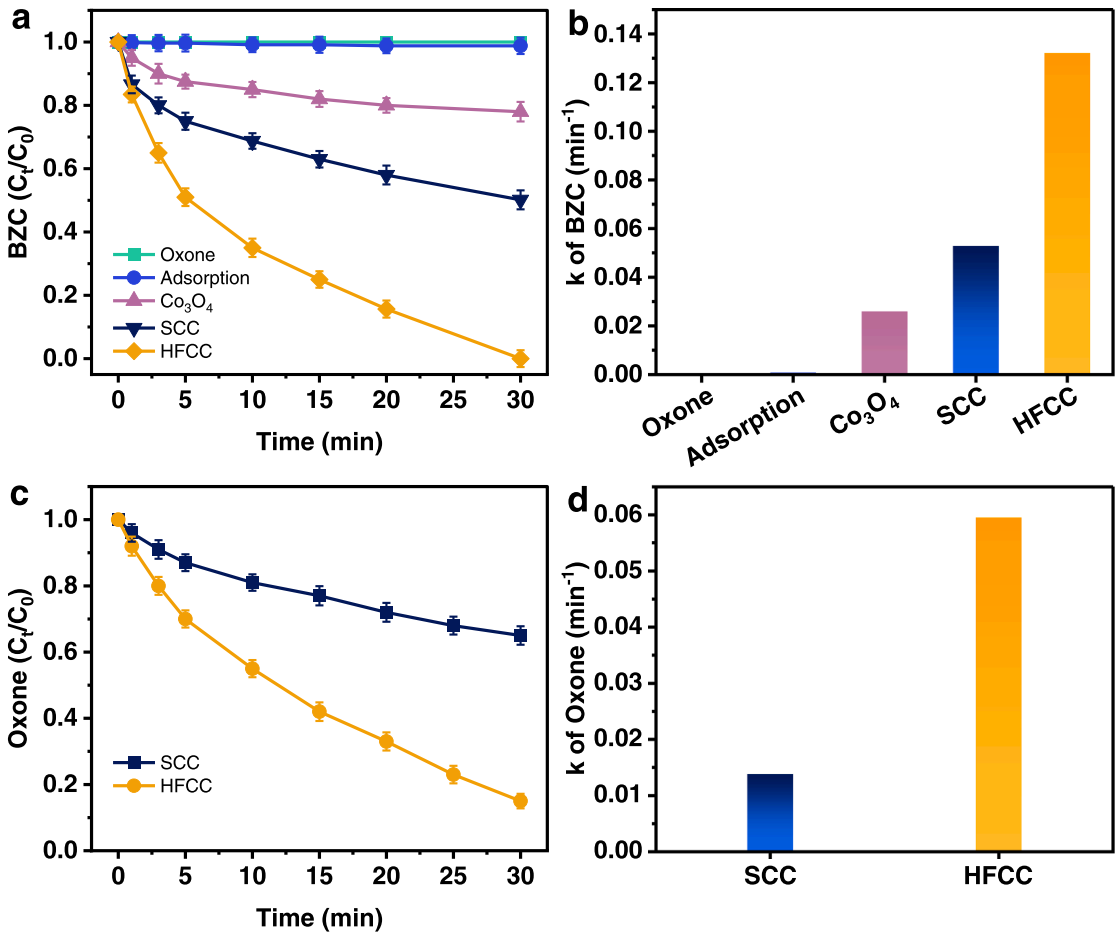

Fig. 3. (a) Comparison of BZC degradation, (b) corresponding rate constants; (c) Oxone consumption, and (d) Oxone consumption rate constants (catalyst = 25 mg/L, Oxone = 200 mg/L, BZC = 10 μM, initial pH = 7, T = 30 °C).

reveals cyclic voltammetry (CV) curves of HFCC and SCC. SCC displayed a relatively small CV curve with less noticeable redox peaks, whereas HFCC obviously showed a larger CV curve with notable redox peaks, validating that HFCC revealed much more superior redox properties and would lead to faster inter-facial processes than SCC [25,26]. Furthermore, the linear sweep voltammograms (LSV) curves of HFCC and were also obtained in Fig. 4(b). At the current density = 5 mA/cm^2, an initial potential of 0.8 V was reached by HFCC, whereas SCC would require a slightly higher initial potential of 0.87 V, demonstrating that the electron transport process in HFCC seemed more effective than in SCC [27]. Moreover, the charge transfers in both of catalysts were also analyzed via their Nyquist plots (Fig. 4c). In comparison to SCC, HFCC showed a considerably smaller semi-circle in the high-frequency region, indicating that HFCC would contain a higher-degree charge transfer with a lower resistance than SCC [28]. These analyses demonstrated that HFCC with the more superior textural properties and more active surfaces would further enable HFCC to possess more advantageous electrochemical behaviors that made HFCC show the considerably higher catalytic activity for Oxone activation to degrade BZC.

Besides, surficial chemistry of heterogeneous catalysts is also the key factor for Oxone activation. As HFCC exhibited a noticeably higher catalytic activity for Oxone activation, it would be insightful to examine surficial chemistry of these catalysts. Herein, X-ray photoelectron spectroscopy analyses of HFCC and SCC were performed as shown in Fig. 4(d–i). In the case of Co 2p in SCC (Fig. 4d), the spectrum consisted of peaks in the range of 780–797 eV. The peaks at 780.1 and 795.2 eV corresponded to Co^{3+}, and the peaks at 781.7 and 797.0 eV would be ascribed to Co^{2+} [29]. Moreover, the O1s spectrum in SCC (Fig. 4f) would be then deconvoluted to show three peaks at 529.6, 531.0, and 532.1 eV, that corresponded to the lattice oxygen (O_L), oxygen vacancy (O_V) and adsorbed oxygen (O_A), respectively [18]. The Co 2p and O 1 s spectra of HFCC were shown in Fig. 4(e and g) and the spectral patterns as well as the deconvoluted peaks were very similar to those in SCC. While the spectral patterns of HFCC and SCC were comparable, respective species fractions might be different and influential to their catalytic activities. To this end, the species of Co^{2+} and Co^{3+}, as well as oxygenic species of HFCC and SCC were then analyzed and summarized in Fig. 4(h and i). Interestingly, the fractions of Co species in HFCC and SCC were actually very close as Co^{2+} and Co^{3+} both accounted for ~50% in HFCC and SCC. Nevertheless, the fractions of oxygen species were considerably different as the fraction of O_V in HFCC (31.9%) was substantially larger than that in SCC (25.6%). Since O_V has been associated with catalytic activities for Oxone activation [30], a higher extent of oxygen vacancies would facilitate electron transfer for inducing activation of Oxone [30]. In addition, the presence of oxygen vacancy with the strong Lewis acidity, would also promote the formation of the singlet oxygen to contribute to the BZC degradation [30]. A higher O_V would lead to a more reactive surface, thereby enabling a larger catalytic activity [31,32]. Thus, the higher fraction of O_V in HFCC might be also an important factor for enabling HFCC to exhibit a higher catalytic activity of Oxone activation than SCC.

These above-mentioned comparisons ascertained that HFCC, derived from the carving-architected treatment, exhibited not only the unique appearance for enhancing its textural properties, but also advantageous surficial characteristics of greater electrochemical properties as well as highly active surfaces, enabling HFCC to be a promising activator for

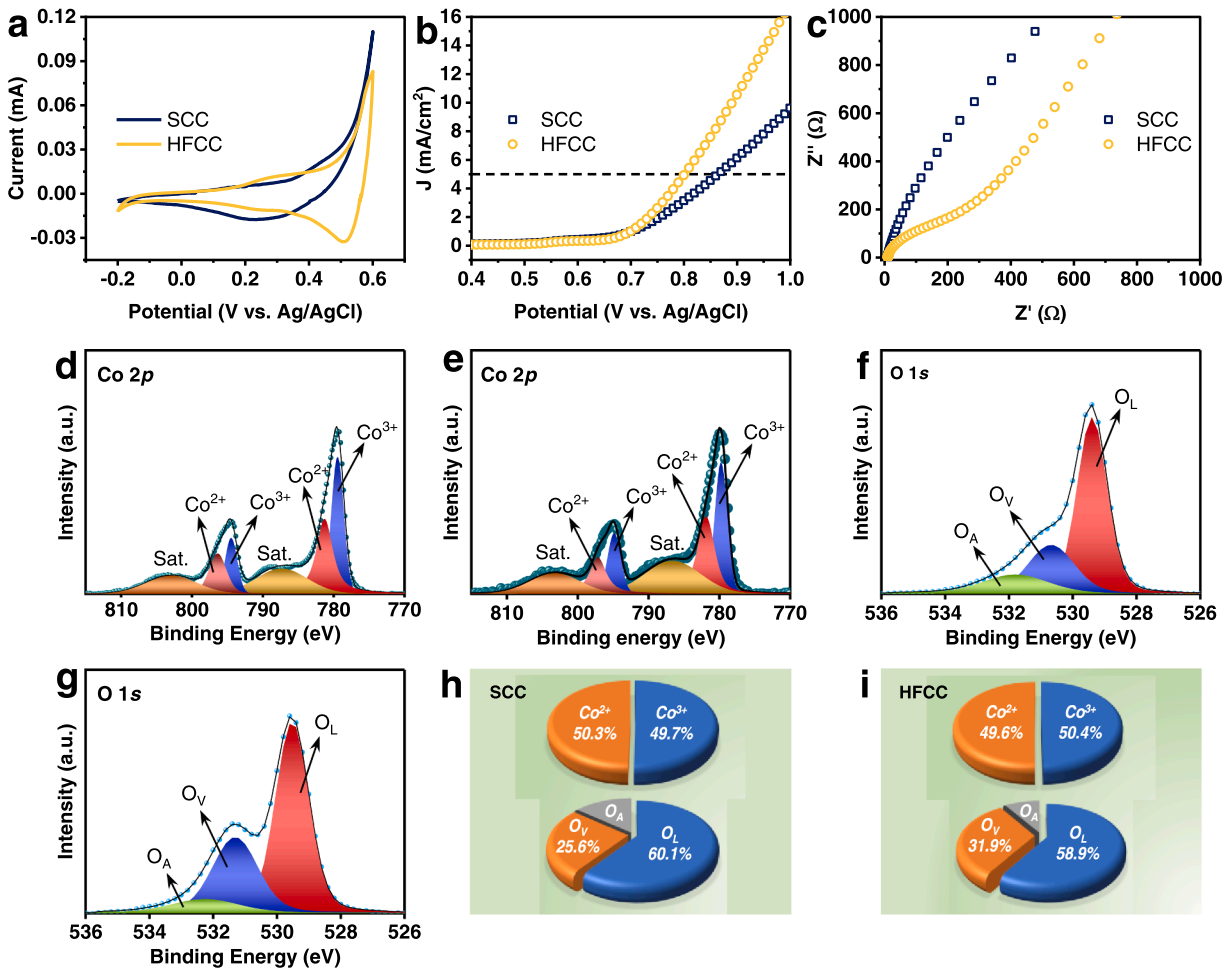

Fig. 4. (a-c) Electrochemical properties of HFCC and SCC: (a) CV curves, (b) LSV curves, (c) EIS Nyquist plots; (d-g) XPS of (d, f) SCC and (e, g) HFCC; (h, i) fractions of species.

Oxone activation in BZC degradation. Other effects (temperature, pH, anions, humic acid) on BZC degradation and the recyclability of HFCC were discussed the Supporting Information.

3.3. Mechanism for BZC degradation

To further realize types of ROS involved during BZC degradation, a series of probe agents would be then examined. Based on reaction rate constants in Table 1, tert-butanol (TBA) is used as a probe agent for $^{\bullet}OH$, whereas methanol (MeOH) can be used for probing the existence of $SO_4^{\bullet-}$ and $^{\bullet}OH$ [33]. Fig. 5(a) displays that when TBA was introduced, BZC degradation proceeded slightly slower and its corresponding rate constant decreased from 0.128 to 0.075 min^{-1}, signifying that $^{\bullet}OH$ might exist and contribute to BZC degradation. When MeOH was introduced, the BZC degradation seemed to inhibited seriously as its k was merely 0.005 min^{-1}, suggesting that both $SO_4^{\bullet-}$ and $^{\bullet}OH$ might simultaneously co-exist during BZC degradation. Besides, another probe agent, benzoquinone (BQ), was employed for examining the existence of superoxide ($O_2^{\bullet-}$). Fig. 5(b) reveals that the presence of BQ also caused BZC degradation to proceed much slowly with a $k = 0.051$ min^{-1}, possibly suggesting that $O_2^{\bullet-}$ might also appear during BZC degradation. Additionally, another probe agent, NaN_3, was adopted to investigate the presence of the non-radical species, singlet oxygen ($^1O_2$), and the introduction of NaN_3 also made BZC degradation proceed relatively slowly with a $k = 0.033$ min^{-1}, signifying that $^1O_2$ also possibly occurred from HFCC/Oxone during BZC degradation, which was involved the non-radical pathway of degradation. To estimate the relative content of ROS contributed to BZC degradation, Eqs. (S13–15) can be used. However, it is found that the inhibitory effect of scavengers is sometimes resulted from enhanced consumption of Oxone rather than from scavenging effect [34,35]. If this is the case, the contribution of ROS will be exaggerated. On the other hand, if the inhibitory effect of scavengers is totally due to the scavenging effect, the increase in the concentration of scavengers will result in higher contribution of ROS. Therefore, the contribution of ROS calculated via quenching experiments might be misleading and thus, it would require more investigations and further studies.

Table 1
2nd order reaction rate constants of various probes with ROS.

Probe	Rate constant ($M^{-1}s^{-1}$)				
	$^{\bullet}OH$	$SO_4^{\bullet-}$	$O_2^{\bullet-}$	$^1O_2$	Ref.
TBA	$3.8–7.6 \times 10^8$	$4.0–9.5 \times 10^5$	–	1.8×10^3	[14,26,36]
MeOH	9.7×10^8	2.5×10^7	–	3.0×10^3	[14,26,36]
BQ	1.2×10^9	–	2.9×10^9	–	[14,26]
NaN_3	1.2×10^{10}	2.52×10^9 (24.4 °C)		1.0×10^9	[14,26,37]
NBT	–	–	$5.76–6.04 \times 10^4$	–	[14,26,38]

To determine actual species of ROS from HFCC/Oxone during BZC degradation, electron spin resonance (EPR) was then adopted by using 5,5-Dimethyl-1-pyrroline N-oxide (DMPO) and 2,2,6,6-

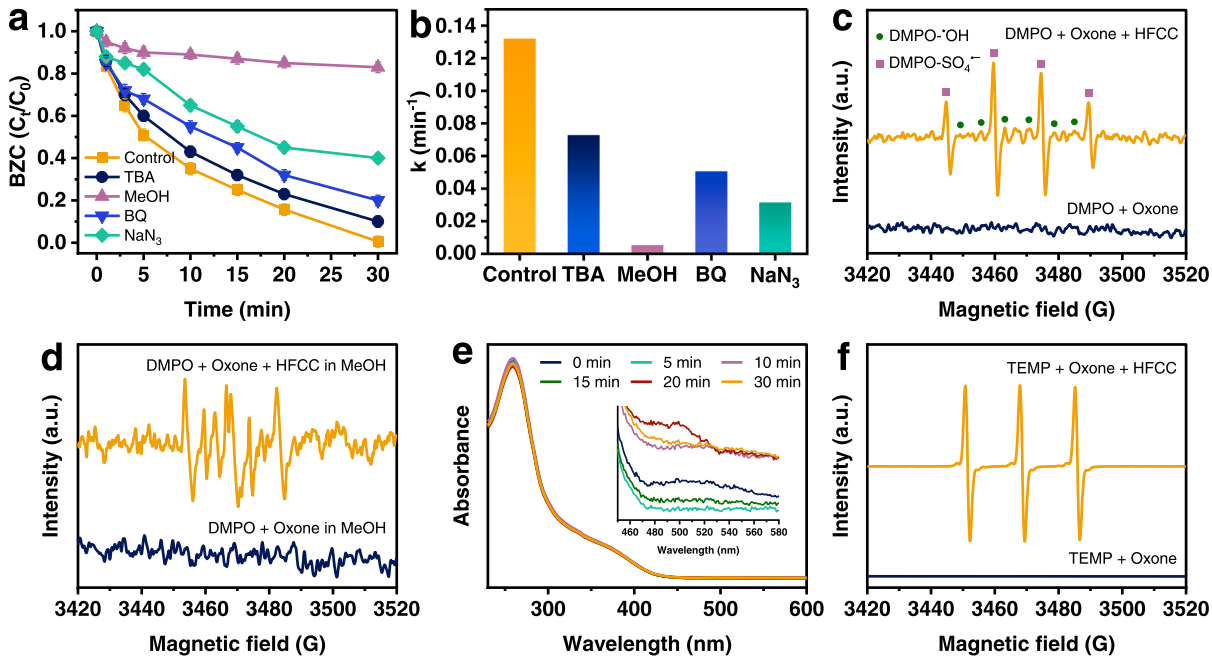

Fig. 5. (a) BZC degradation under effect of scavengers, (b) corresponding rate constants, (c) EPR spectra of DMPO-$SO_4^{\bullet-}$/$^{\bullet}OH$ signals, (d) EPR spectra of DMPOX signal, e) determination of superoxide by NBT reduction UV–vis spectra, and (f) EPR spectra of TMP-$^1O_2$ signal (catalyst = 25 mg/L, Oxone = 200 mg/L, BZC = 10 μM, initial pH = 7, T = 30 °C).

tetramethylpiperidine (TMP) as spin-trapping agents [39]. Fig. 5(c) reveals that when DMPO was introduced in the absence of HFCC, no obvious pattern was observed. Nevertheless, as DMPO, Oxone, and HFCC were present simultaneously, a distinct pattern was then observed and ascribed to DMPO-$SO_4^{\bullet-}$ and DMPO-$^{\bullet}OH$ [40]. This ascertains that both $SO_4^{\bullet-}$ and $^{\bullet}OH$ were generated from HFCC/Oxone, contributing to BZC degradation. Moreover, the same measurement was then performed in methanol to examine whether the superoxide, $O_2^{\bullet-}$, would be produced from HFCC/Oxone. While almost no signal was observed in the case of DMPO and Oxone in methanol, a notable signal could be detected in the case of DMPO, Oxone and HFCC in methanol (Fig. 5d). However, the signal was considered as 5,5-dimethylpyrroline-(2)-oxyl-(1) (DMPOX) rather than the signal of DMPO—$O_2^{\bullet-}$. The formation of DMPOX was possibly due to the oxidation of DMPO by $^1O_2$ as the reaction rate between methanol and $^1O_2$ was quite low (3.0×10^3 $M^{-1}s^{-1}$ [36]). This result suggests that no significant amount of $O_2^{\bullet-}$ was present during BZC degradation. To further explore the existence of $O_2^{\bullet-}$, UV–vis spectra of nitro blue tetrazolium (NBT) were recorded as NBT could be reduced specifically by $O_2^{\bullet-}$ (k = 5.76–6.04×10^4 $M^{-1}s^{-1}$) to monoformazan, absorbing the visible light at 530 nm [14,18,20,26,37]. Nonetheless, Fig. 5(e) displays that when NBT was introduced to BZC degradation as the peaks at 259 and 330 nm were attributed to NBT itself, the spectral variation did not show noticeable bands of monoformazan at 530 nm, indicating insignificant existence of $O_2^{\bullet-}$.

In the earlier section, we observed that the introduction of BQ slightly inhibited BZC degradation. This phenomenon has been also observed in literatures because when $O_2^{\bullet-}$ was insignificant, the addition of BQ might consume a part of Oxone without generating ROS, thereby intervening with BZC degradation [41].

On the other hand, when the trapping agent, TMP, was employed, almost no noticeable signal was observed in the case of TMP and Oxone (Fig. 5f). However, once TMP, Oxone and HFCC were introduced simultaneously, a distinct pattern of triplet was then observed and ascribed to TMP-$^1O_2$ signal (TMPN), confirming that $^1O_2$ certainly existed and contributed to BZC degradation via the non-radical pathway. These analyses also corroborated that BZC degradation by HFCC/Oxone was certainly involved with a series of ROS ($SO_4^{\bullet-}$, $^{\bullet}OH$, $^1O_2$).

3.4. BZC degradation pathway and eco-toxicity evaluation

Since HFCC can efficiently activated Oxone to degrade BZC, it would be crucial to further investigate the BZC degradation process especially given that no studies of BZC degradation by SR-based COTs has ever been investigated. For exploring the BZC degradation pathway by ROS, the computational chemistry using the Density Function Theory (DFT) was adopted to investigate the molecular susceptibility in BZC [18]. The molecular structure of BZC was be geometrically-optimized as shown in Fig. 6(a). Accordingly, Fig. 6(b) also illustrates the electrostatic potential (ESP)-mapped isosurface of BZC, which indicates that the electron-rich region (the reddish and orange zones) of BZC would be prone to electrophilic reactions [26]. Fig. 6(c and d) display the highest occupied molecular orbital (HOMO) and the lowest unoccupied molecular orbital (LUMO) of BZC. In general, the HOMO regions would attract electrophilic attacks, and both $SO_4^{\bullet-}$ and $^{\bullet}OH$ are considered to exhibit electrophilic nature and $^1O_2$ is a strongly electrophilic species. Therefore, the HOMO located at the benzene ring of BZC seemed to easily receive electrophilic attacks from these ROS [14].

To further distinguish the most probable sites of BZC for gaining attacks, the Fukui index distribution of BZC were then mapped (Fig. 6e-g) and the values were summarized in Fig. 6(h). In particular, f^-, f^0, and f^+ represent the electrophilic attack, the radical attack, and the nucleophilic attack, respectively. Since $^1O_2$ is a highly reactive electrophilic species, sites of BZC with relatively high and positive values of f^- would tend to receive the electrophilic attacks. Specifically, 2O, 3 N, 4C, 8C, and 9C have relatively high f^- values, suggesting that these sites might undergo the electrophilic attacks. On the other hand, the sites with high values of f^0 would tend to receive the radical attacks, such as 2O, 3 N, 4C, and 10C. These analyses indicate that 2O, 3 N and 4C might be more susceptible to attacks of ROS during BZC degradation by HFCC/Oxone. In addition, the possible attack sites of OH^-, a nucleophile in the solution, are assessed by f^+. Consequently, f^+ values of 2O, 3 N, 5C, 6C, 7C, and 10C are high. These sites, therefore, easily undergo hydroxylation [26].

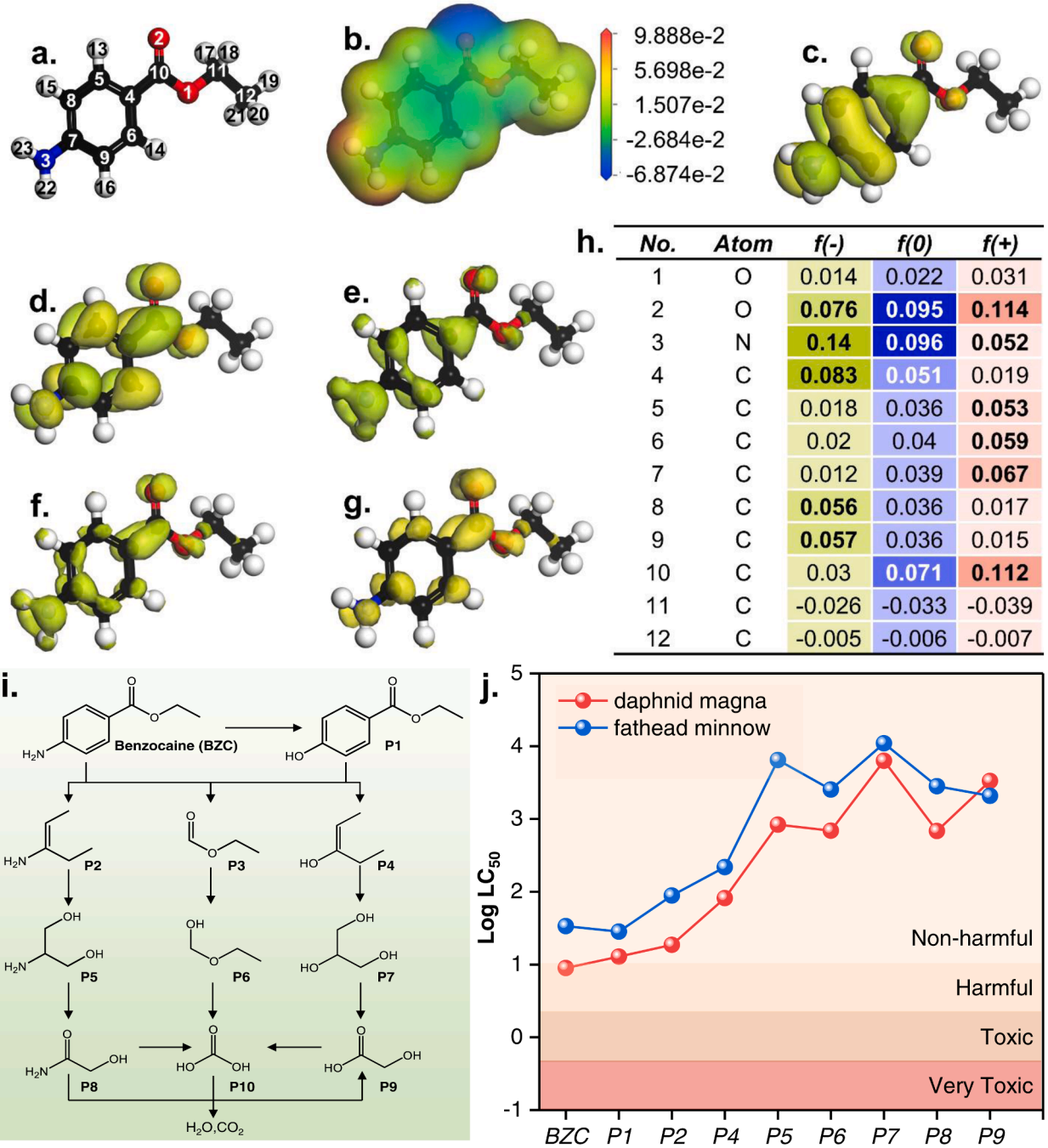

No.	Atom	f(-)	f(0)	f(+)
1	O	0.014	0.022	0.031
2	O	**0.076**	**0.095**	**0.114**
3	N	**0.14**	**0.096**	**0.052**
4	C	**0.083**	0.051	0.019
5	C	0.018	0.036	**0.053**
6	C	0.02	0.04	**0.059**
7	C	0.012	0.039	**0.067**
8	C	**0.056**	0.036	0.017
9	C	**0.057**	0.036	0.015
10	C	0.03	**0.071**	**0.112**
11	C	-0.026	-0.033	-0.039
12	C	-0.005	-0.006	-0.007

Fig. 6. DFT calculation for BZC: (a) the optimized molecule structure, (b) electrostatic potential (ESP), (c) HOMO; (d) LUMO; (e-g) condensed Fukui index distribution for (e) electrophilic attack (f^-), (f) radical attack (f^0), (g) nucleophilic attack (f^+); (h) a summary of Fukui indices; (i) proposed degradation process of BZC based on the detected intermediates; and (j) eco-toxicity evaluation by the Toxicity Estimation Software Tool (the toxicities of P3 and P10 are not available in the T.E.S.T database).

To determine the degradation pathway of BZC by HFCC/Oxone, the mass spectrometry of degradation products from BZC degradation (Fig. S8 and Table S2) was then analyzed and combined with the above-mentioned theoretical knowledge to propose the degradation process in Fig. 6(i).

In the beginning, the primary amine group of BZC might be substituted by a hydroxyl group to form an initial intermediate, P1. Subsequently, both BZC and P1 might be attacked at the connecting site between the benzene ring and formate group to break the structure. Therefore, BZC might be decomposed to afford P2 and P3 after the breakage. The intermediate, P2, would then be oxidized to produce P5, which could be further oxidized to generate P8. On the other hand, the intermediate, P3, would be then transformed to P6, which might be further oxidized to produce P10. Simultaneously, P8 might also be oxidized to produce P10 as well as P9 by substituting the amine group with the hydroxyl group. Moreover, the initial intermediate, P1, could be also oxidized to produce P4 and P3 due to the breakage. P4 would be then oxidized to generate P7, and then P9, which might be degraded to result in P10. Eventually, these low-molecular-weight compounds would be decomposed and mineralized to CO_2 and H_2O.

In view of the degradation pathway of BZC by HFCC/Oxone, it was also crucial to evaluate the eco-toxicity of intermediates generated from

BZC degradation especially for aquatic life. Herein, the Toxicity Estimation Software Tool (T.E.S.T.) from the United States Environmental Protection Agency was adopted to evaluate acute toxicities (LC50) of these intermediates towards daphnid magna and fathead minnow. Based on the Globally Harmonized System of Classification and Labeling of Chemicals (Table S3), the data of LC50 of these intermediates from the T.E.S.T. could be then categorized into the four levels of toxicity (i.e., very toxic, toxic, harmful and non-harmful). Fig. 6(j) displays values of Log LC50 of these intermediates as well as their categories. In the case of daphnid magna, the toxicity of pristine BZC was relatively high (i.e., very low dosage of LC50). As BZC was decomposed, the toxicities of the initial intermediates (P1 and P2) seemed to decrease gradually, and then toxicities were significantly reduced in P4~P9. Similarly, the same tendency was also observed in the case of fathead minnow as the initial toxicity of BZC was high, and gradually decreased along the decomposition process. These results suggest that while BZC could be considered as a harmful chemical, its degradation intermediates by HFCC/Oxone were mostly non-harmful, demonstrating that HFCC/Oxone was useful to degrade BZC without the formation of toxic and very toxic by-products, and also detoxify BZC along the decomposition.

4. Conclusion

Herein, the HFCC with the hollow-engineered fluffy nanostructured Co_3O_4 was successfully prepared through the facile but convenient carving-architected treatment using CoMOF as a precursor. In comparison to SCC, the solid (non-hollow) Co_3O_4 from the calcination of CoMOF, HFCC exhibited not only the interesting morphology for enhancing textural properties, but also useful surface properties of outstanding electrochemical properties as well as highly reactive surfaces, enabling HFCC to possess the substantially higher activities than SCC and traditional Co_3O_4 NP for activating Oxone in degrading BZC. These advantageous features make HFCC a promising heterogeneous catalyst for activating Oxone to eliminate BZC and other emerging contaminants in water.

Declaration of Competing Interest

The authors declare that they have no known competing financial interests or personal relationships that could have appeared to influence the work reported in this paper.

Supplementary materials

Supplementary material associated with this article can be found, in the online version, at doi:10.1016/j.jtice.2023.105042.

References

[1] Gago-Ferrero P, Bletsou AA, Damalas DE, Aalizadeh R, Alygizakis NA, Singer HP, Hollender J, Thomaidis NS. Wide-scope target screening of >2000 emerging contaminants in wastewater samples with UPLC-Q-ToF-HRMS/MS and smart evaluation of its performance through the validation of 195 selected representative analytes. J Hazard Mater 2020;387:121712.

[2] Jiang R, Lu G, Yan Z, Wu D, Zhou R, Bao X. Insights into a CQD-SnNb2O6/BiOCl Z-scheme system for the degradation of benzocaine: influence factors, intermediate toxicity and photocatalytic mechanism. Chem Eng J 2019;374:79–90.

[3] Kudlek E. Decomposition of contaminants of emerging concern in advanced oxidation processes. Water 2018;10:955.

[4] Richardson N, Meakin B. The influence of temperature on the sorption of benzocaine by nylon 6 from aqueous cosolvents. J Pharm Pharmacol 1977;29:86–8.

[5] Howe G, Bills T, Marking L. Communications: removal of benzocaine from water by filtration with activated carbon. Progress Fish Cult 1990;52:32–5.

[6] Kohantorabi M, Moussavi G, Giannakis S. A review of the innovations in metal- and carbon-based catalysts explored for heterogeneous peroxymonosulfate (PMS) activation, with focus on radical vs. non-radical degradation pathways of organic contaminants. Chem Eng J 2021;411:127957.

[7] Hassani A, Eghbali P, Mahdipour F, Wacławek S, Lin KYA, Ghanbari F. Insights into the synergistic role of photocatalytic activation of peroxymonosulfate by UVA-LED irradiation over CoFe2O4-rGO nanocomposite towards effective Bisphenol A degradation: performance, mineralization, and activation mechanism. Chem Eng J 2023;453:139556.

[8] Khiem TC, Duan X, Liu WJ, Park YK, Bui HM, Oh WD, Ghotekar S, Tsang YF, Lin KYA. MOF-templated hollow cobalt sulfide as an enhanced Oxone activator for degradation of UV Absorber: key role of sulfur Vacancy-Induced highly active CoII sites. Chem Eng J 2023;453:139699.

[9] Liu WJ, Kwon E, Huy NN, Khiem TC, Lisak G, Wi-Afedzi T, Wu CC, Ghanbari F, Lin KYA. Facilely-prepared sulfide-doped Co_3O_4 nanocomposite as a boosted catalyst for activating Oxone to degrade a sunscreen agent. J Taiwan Inst Chem Eng 2022;133:104253.

[10] Khiem TC, Tuan DD, Kwon E, Thanh BX, Tsang YF, Munagapati VS, Wen JC, Hu C, Lin KYA. Hollow and oval-configured ultrafine Co_3O_4 as a highly-efficient activator of monopersulfate for catalytic elimination of Azorubin S. Sustain Environ Res 2022;32:48.

[11] Liu WJ, Kwon E, Huy NN, Khiem TC, Lisak G, Wi-Afedzi T, Wu CC, Ghanbari F, Lin KYA. Facilely-prepared sulfide-doped Co_3O_4 nanocomposite as a boosted catalyst for activating Oxone to degrade a sunscreen agent. J Taiwan Inst Chem Eng 2022;133.

[12] Yin JY, Kwon E, Thanh BX, Lisak G, Oh WD, Lin KYA. Cobalt sulfide nanosheets derived from sulfurization of Prussian blue analogue as an enhanced catalyst for activating monopersulfate to degrade caffeine. J Taiwan Inst Chem Eng 2021;123:115–23.

[13] Deng J, Feng S, Zhang K, Li J, Wang H, Zhang T, Ma X. Heterogeneous activation of peroxymonosulfate using ordered mesoporous Co_3O_4 for the degradation of chloramphenicol at neutral pH. Chem Eng J 2017;308:505–15.

[14] Khiem TC, Huy NN, Trang TD, Wen JC, Kwon E, Chang HC, et al. Boosting elimination of sunscreen, tetrahydroxybenzophenone (BP-2), from water using monopersulfate activated by thorny NanoBox of Co@ C prepared via the engineered etching strategy: a comparative and mechanistic investigation. Chemosphere 2023;327:138469.

[15] Tuan DD, Khiem C, Kwon E, Tsang YF, Sirivithayapakorn S, Thanh BX, Lisak G, Yang H, Lin KYA. Hollow porous cobalt oxide nanobox as an enhanced for activating monopersulfate to degrade 2-hydroxybenzoic acid in water. Chemosphere 2022;294:133441.

[16] Lin KYA, Chen BC. Efficient elimination of caffeine from water using Oxone activated by a magnetic and recyclable cobalt/carbon nanocomposite derived from ZIF-67. Dalton Trans 2016;45:3541–51.

[17] Tao J, Xu L, Wan L, Hou J, Yi P, Chen P, Zhou J, Yao Z. Cubic-like Co/NC composites derived from ZIF-67 with a dual control strategy of size and graphitization degree for microwave absorption. Nanoscale 2021;13:12896–909.

[18] Khiem TC, Tuan DD, Kwon E, Huy NN, Oh WD, Chen WH, Lin KYA. Degradation of dihydroxybenzophenone through monopersulfate activation over nanostructured cobalt ferrites with various morphologies: a comparative study. Chem Eng J 2022;450:137798.

[19] Wang Y, Wei X, Hu X, Zhou W, Zhao Y. Effect of formic acid treatment on the structure and catalytic activity of Co_3O_4 for N_2O decomposition. Catal Lett 2019;149:1026–36.

[20] Khiem TC, Mao PH, Park YK, Duan X, Thanh BX, Hu C, et al. Templating agent-mediated Cobalt oxide encapsulated in Mesoporous silica as an efficient oxone activator for elimination of toxic anionic azo dye in water: mechanistic and DFT-assisted investigations. Chemosphere 2022;313:137309.

[21] Khiem TC, Tuan DD, Kwon E, Thanh BX, Tsang YF, Munagapati VS, Wen JC, Hu C, Lin KYA. Hollow and oval-configured ultrafine Co3O4 as a highly-efficient activator of monopersulfate for catalytic elimination of Azorubin S. Sustain Environ Res 2022;32:1–15.

[22] Zhang Q, Mo S, Chen B, Zhang W, Huang C, Ye D. Hierarchical Co_3O_4 nanostructures in-situ grown on 3D nickel foam towards toluene oxidation. Mol Catal 2018;454:12–20.

[23] Diallo A, Beye AC, Doyle TB, Park E, Maaza M. Green synthesis of Co_3O_4 nanoparticles via Aspalathus linearis: physical properties. Green Chem Lett Rev 2015;8:30–6.

[24] Wang Z, Wang W, Zhang L, Jiang D. Surface oxygen vacancies on Co_3O_4 mediated catalytic formaldehyde oxidation at room temperature. Catal Sci Technol 2016;6:3845–53.

[25] Cong Khiem T, Duan X, Liu WJ, Park YK, Manh Bui H, Oh WD, et al. MOF-templated hollow Cobalt sulfide as an enhanced Oxone activator for degradation of UV absorber: key role of sulfur vacancy-induced highly active CoII sites. Chem Eng J 2022;453:139699.

[26] Khiem TC, Huy NN, Kwon E, Duan X, Wacławek S, Bedia J, et al. Hetero-interface-engineered sulfur vacancy and oxygen doping in hollow Co_9S_8/Fe_7S_8 nanospheres towards monopersulfate activation for boosting intrinsic electron transfer in paracetamol degradation. Appl Catal B 2023;330:122550.

[27] Mao PH, Khiem TC, Kwon E, Chang HC, Bui HM, Duan X, Yang H, Ghotekar S, Chen WH, Tsai YC. Ambient-visible-light-mediated enhanced degradation of UV stabilizer bis (4-hydroxyphenyl) methanone by nanosheet-assembled cobalt titanium oxide: a comparative and DFT-assisted investigation. Water 2022;14:3318.

[28] Li Y, Li FM, Meng XY, Li SN, Zeng JH, Chen Y. Ultrathin Co_3O_4 nanomeshes for the oxygen evolution reaction. ACS Catal 2018;8:1913–20.

[29] Li BC, Yang H, Kwon E, Tuan DD, Khiem TC, Lisak G, Thanh BX, Ghanbari F, Lin KYA. Catalytic reduction of bromate by Co-embedded N-doped carbon as a magnetic Non-noble metal hydrogenation catalyst. Sep Purif Technol 2021;277:119320.

[30] Guo S, Liu M, You L, Cheng G, Li J, Zhou K. Oxygen vacancy induced peroxymonosulfate activation by Mg-doped Fe_2O_3 composites for advanced oxidation of organic pollutants. Chemosphere 2021;279:130482.

[31] Tsai YC, Huy NN, Lee J, Lin YF, Lin KYA. Catalytic soot oxidation using hierarchical cobalt oxide microspheres with various nanostructures: insights into relationships of morphology, property and reactivity. Chem Eng J 2020;395:124939.
[32] Liu WJ, Wang H, Lee J, Kwon E, Thanh BX, You S, Park YK, Tong S, Lin KYA. Investigating crystal plane effect of Co_3O_4 with various morphologies on catalytic activation of monopersulfate for degradation of phenol in water. Sep Purif Technol 2021;276:119368.
[33] Liu WJ, Kwon E, Thanh BX, Khiem TC, Tuan DD, Lin JY, Wi-Afedzi T, Hu C, Sirivithayapakorn S, Lin KYA. Hofmann-MOF derived nanoball assembled by FeNi alloy confined in carbon nanotubes as a magnetic catalyst for activating peroxydisulfate to degrade an ionic liquid. Sep Purif Technol 2022;295:120945.
[34] Zhou Y, Jiang J, Gao Y, Ma J, Pang SY, Li J, Lu XT, Yuan LP. Activation of peroxymonosulfate by benzoquinone: a novel nonradical oxidation process. Environ Sci Technol 2015;49:12941–50.
[35] Yun ET, Lee JH, Kim J, Park HD, Lee J. Identifying the nonradical mechanism in the peroxymonosulfate activation process: singlet oxygenation versus mediated electron transfer. Environ Sci Technol 2018;52:7032–42.
[36] Yang Y, Banerjee G, Brudvig GW, Kim JH, Pignatello JJ. Oxidation of organic compounds in water by unactivated peroxymonosulfate. Environ Sci Technol 2018;52:5911–9.
[37] Khiem TC, Duan X, Liu WJ, Park YK, Bui HM, Oh WD, et al. MOF-templated hollow cobalt sulfide as an enhanced Oxone activator for degradation of UV absorber: key role of sulfur vacancy-induced highly active CoII sites. Chem Eng J 2022;453:139699.
[38] Bielski BH, Shiue GG, Bajuk S. Reduction of nitro blue tetrazolium by CO_2-and O_2-radicals. J Phys Chem 1980;84:830–3.
[39] Liu WJ, Yang H, Park YK, Kwon E, Huang CW, Thanh BX, Khiem TC, You S, Ghanbari F, Lin KYA. Enhanced degradation of ultra-violet stabilizer Bis (4-hydroxy) benzophenone using oxone catalyzed by hexagonal nanoplate-assembled CoS 3-dimensional cluster. Chemosphere 2022;288:132427.
[40] Liu WJ, Kwon E, Thanh BX, Khiem TC, Lisak G, Lee J, Lin KYA. 3D hexagonal hierachitectured cobalt sulfide as an enhanced catalyst for activating monopersulfate to degrade sunscreen agent ensulizole. J Taiwan Inst Chem Eng 2022;131:104109.
[41] Cong Khiem T, Dinh Tuan D, Kwon E, Nhat Huy N, Oh WD, Chen WH, Lin KYA. Degradation of dihydroxybenzophenone through monopersulfate activation over nanostructured cobalt ferrites with various morphologies: a comparative study. Chem Eng J 2022;450:137798.